Enhanced resonance energy transfer in gold nanoparticles bifunctionalized by tryptophan and riboflavin and its application in fluorescence bioimaging

Jelena Pajović, Radovan Dojčilović, Slávka Kaščáková, Matthieu Réfrégiers, Dušan Božanić, Vladimir Djoković

Highlights

Enhanced resonance energy transfer in gold nanoparticles bifunctionalized by tryptophan and riboflavin and its application in fluorescence bioimaging

Jelena D. Pajović, Radovan J. Dojčilović, Slávka Kaščáková, Matthieu Réfrégiers, Dušan K. Božanić, Vladimir Djoković

- Gold nanoparticles are functionalized by tryptophan and riboflavin (ATR).
- In ATR, the biomolecular pair exhibits pronounced resonance energy transfer.
- Human liver cancer (Huh) cells were incubated with ATR nanosystem.
- The energy transfer in ATR affects the photobleaching (PB) rates of biomolecules.
- The change in PB rates enables localization of ATR in Huh by fluorescence imaging.

Enhanced resonance energy transfer in gold nanoparticles bifunctionalized by tryptophan and riboflavin and its application in fluorescence bioimaging

Jelena D. Pajović[a,b], Radovan J. Dojčilović[c,d,e], Slávka Kaščáková[f,g], Matthieu Réfrégiers[a,h], Dušan K. Božanić[c,d,*], Vladimir Djoković[c,d,*]

[a]*DISCO beamline, Synchrotron SOLEIL, BP 48, Gif sur Yvette, 91192, France*
[b]*University of Belgrade, Faculty of Physics, Studentski trg 12, Belgrade, 11001, Serbia*
[c]*"VINČA" Institute of Nuclear Sciences - National Institute of the Republic of Serbia, University of Belgrade, PO Box 522, Belgrade, 11001, Serbia*
[d]*Centre of excellence for photoconversion, P.O. Box 522, Belgrade, 11001, Serbia*
[e]*Department of Experimental and Health Sciences, Pompeu Fabra University, Carrer del Dr. Aiguader 88, Barcelona, 08003, Spain*
[f]*Inserm, Unité 1193, Villejuif, F-94800, France*
[g] *University Paris-Sud XI, UMR-S1193, Villejuif, F-94800, France*
[h]*Centre de Biophysique Moléculaire, CNRS UPR4301, Rue Charles Sadron, Orléans, 45071, France*

Abstract

Gold nanoparticles were functionalized by amino acid tryptophan and vitamin riboflavin - a resonance energy transfer (RET) pair of biomolecules. The presence of the gold nanoparticles resulted in 65% increase in RET efficiency. Because of enhanced RET efficiency, the photobleaching dynamics of the fluorescent molecules at the surface of the nanoparticles is different from that of molecules in solution. The observed effect was used for detection of the functionalized nanoparticles within biological material rich with autofluorescent species. Synchrotron radiation deep-ultraviolet fluorescence microscopy is used to study the photobleaching dynamics of the fluorescence centers within human hepatocellular carcinoma Huh7.5.1 cells incubated with the nanoparticles. The fluorescent centers were classified according to their photobleaching dynamics, which enabled the discrimination of the cell areas where the accumulation

*Corresponding authors
Email addresses: jelena@ff.bg.ac.rs (Jelena D. Pajović), bozanic@vin.bg.ac.rs (Dušan K. Božanić), djokovic@vin.bg.ac.rs (Vladimir Djoković)

of the nanoparticles takes place, even though the particles were smaller than the spatial resolution of the images.

Keywords: gold nanoparticles, fluorescence imaging, resonance energy transfer, photobleaching, tryptophan, riboflavin

1. Introduction

Gold nanoparticles (Au NPs) are one of the most studied nanosystems [1, 2, 3, 4, 5, 6]. They are especially suitable for application in bionanotechnology and nanomedicine due to their chemical stability and biocompatibility [3, 7]. Au NP exhibit surface plasmon resonant absorption in the visible part of the electromagnetic spectrum, while the position of the resonance is sensitive to the environmental changes [8]. This enables monitoring of the nanoparticle interactions with biological molecules using optical spectroscopy. The adsorption of various biomolecules onto the surface of Au NPs is also a good path for the fabrication of complex nanosystems with desired properties [9, 10]. Functionalized Au NPs have been applied in different fields of biotechnology and medicine, including sensing [11, 12, 6] and microscopy [13, 14], as well as photothermal [15], radio- [16], and photodynamic [17, 18] therapies of cancer.

Information on spatial distribution of Au NP within a biological system is of importance for understanding of their biological activity. So far, structural techniques such as transmission electron microscopy [19], as well as noninvasive optical methods that include surface-enhanced Raman scattering, Rayleigh light scattering and confocal Raman microscopy [1], were used to investigate the nanoparticle-cell interactions and the migration of nanoparticles in cells. Our recent results demonstrated that synchrotron radiation deep-ultraviolet (DUV) fluorescence microscopy is a convenient method for determination of the accumulation of antibiotics [20, 21, 22, 23, 24], and nanoparticles [25, 26, 27, 28, 29] within an individual cell with a spatial resolution of $\sim$150 nm. For example, DUV fluorescent imaging studies of bacteria incubated with tryptophan functionalized silver [27] and gold [29] nanoparticles and showed that it was possible to distinguish the fluorescent signals of the nanostructures from the autofluorescence of the cells, due to a relatively simple morphology and small size ($\sim 3\,\mu$m) of these prokaryotic cells.When it comes to more complex cells, such as human tissue cells, the signal differentiation is far from a trivial since the biomaterial is highly heterogeneous. In an attempt to localize the fluorescent signal that comes from the nanoparticles, we used

a novel approach and followed the photobleaching of the fluorescent centers in human hepatocellular carcinoma Huh7.5.1 cells.

This study is focused on Au NP functionalized by both tryptophan and riboflavin, a resonance energy transfer (RET) pair of molecules, and the investigation of the RET efficiency in these hybrid nanosystems. RET is a dipole-dipole interaction process that occurs between a molecule in an excited state (donor) and a molecule in the ground state (acceptor), if the fluorescence band of the donor overlaps the excitation band(s) of the acceptor [30, 31, 32, 33]. It was shown that RET efficiency for a pair of molecules can be affected by the metal surface [34, 35, 36, 37, 38, 39, 40, 41, 42], which has been extensively studied both theoretically and experimentally. However, there is no general consensus on the role of metal on RET process, mainly due to different basic systems used in theoretical and experimental studies [43]. Theoretical investigations usually assume bare metal nanoparticles [44, 45, 39, 40, 37, 38] and a single RET pair of the fluorophores placed at some distance from the metallic surface, while in most of experimental studies [46, 47, 36], there are intermediate linkers between particles surfaces and fluorophores. In the present study, we used the simple chemical procedure for the fabrication of bare Au NP that were directly functionalized by tryptophan and riboflavin, i. e. without the use of intermediate ligands. In this way it was possible to study the effects of the metal surface on RET process directly.

An important consequence of RET is that it changes photobleaching dynamics of the donor molecule by providing additional channel for the deexcitation. This effect is the basis for photobleaching RET imaging [48]. It will be shown that the Au NPs change the efficiency of RET between tryptophan and riboflavin and, consequently, affect the photobleaching dynamics further of the donor molecules. Our aim is to exploit this effect in order to detect the functionalized nanoparticles in human cancer cells. It is important to emphasize that we use biomolecules, which are common in biological systems. Moreover, tryptophan is often chosen as a donor molecule in RET studies related to microorganisms or tissues [30], while riboflavin is a vitamin critical in oxidation and reduction processes in cells. They both contribute to the autofluorescence of the cells and are responsible for photochemical sensitivity of the biological material. Therefore, this study also shows that it is possible to distinguish between these biomolecules that are attached to Au NP and those that are already present in cells by using standard optical techniques. This approach is in the line with current trends presented in a recent review by Sahl, Hell and Jakobs [49] on fluorescence nanoscopy.

They suggested the use of certain physical processes as the auxiliary tools in attempts to break the diffraction barrier, i. e. to increase our ability to differentiate between nanoobjects and particular molecules in cells.

2. Materials and methods

2.1. Materials

Gold(III)chloride trihydrate $HAuCl_4 \times 3H_2O$ ($\geq$99.9% trace metals basis), sodium borohydride $NaBH_4$ (powder $\geq$98%) , L-tryptophan, Trp, ($\geq$98%) and (-)-Riboflavin, Rb, ($\geq$98%) were purchased from Sigma Aldrich and used as received. 4D ultrapure water was used in all synthesis procedures.

2.2. Preparation of bifunctionalized gold nanoparticles

Gold nanoparticles (Au NPs) were prepared by chemical reduction of chloroaurate ions by a strong reducing agent, as explained elsewhere [29]. Briefly, in a typical procedure, 25 mg of sodium borohydride was added rapidly to 100 ml of 0.2 mM $HAuCl_4 \times 3H_2O$ aqueous solution under vigorous stirring at room temperature for one hour and stored in opaque vials in cold. If kept in the dark at 4 °C, the obtained Au NPs were chemically stable for months after the preparation.

For the functionalization of gold nanoparticles, batch aqueous solutions of Trp and Rb were prepared in concentrations of 10 mM and 0.25 mM, respectively, and added to the gold colloid in the desired molar ratio while stirring. Gold to tryptophan molar ratio was kept at 1:2, while gold to riboflavin ratios were varied from 0.25 to 1 with steps of 0.25. The functionalization procedure assumed rigorous stirring of the mixtures for 1 h at room temperature. The notation of the colloidal and control samples, as well as the amount of the chemicals used in their preparation, are listed in Table S1 in the Supplementary Information. The reported concentrations of gold in colloid concerns gold atoms.

In order to remove unbound molecules from the colloid particles, the samples are purified by centrifugation. The centrifugation process was carried out at 40 000 rpm (111 000×g) for 20 minutes at 4°C under low vacuum. Supernatants, which included 80% of the initial centrifuged volume, were disposed of. The obtained pellets were submerged in an ultrasound bath for 15 s, transferred to glass vials and stored at 4°C in dark. These samples are used for the incubation of the human hepatocellular carcinoma-derived cell

line. For the optical characterization, however, the purified functionalized colloids were diluted to the stated concentrations.

2.3. Characterization of bifunctionalized gold nanoparticles

The size and morphology of functionalized gold nanoparticles were investigated by transmission electron microscopy (TEM) using a TECNAI F30 G2 Twin transmission electron microscope operating at 300 kV. The obtained resolution was 0.205 nm. The samples were deposited on carbon-coated copper grids and dried at room temperature, at their initial concentrations. The size distribution of the nanoparticles was determined by measuring diameters of circular areas of more than 260 nanoparticles.

The absorbance spectra of colloidal and biomolecule solutions in water were carried out on a Thermo Evolution 600 spectrophotometer.

The photoluminescence spectra of the pure solutions of the biomolecules and the functionalized colloids in water were recorded on a PerkinElmer LS45 fluorescence spectrophotometer, at a 290 nm excitation wavelength. A numerical procedure was used to correct data for the contribution of the second harmonic band to the obtained spectra.

2.4. Cell culture and preparation of biological samples

Human hepatocellular carcinoma-derived Huh7.5.1 cells were cultured as monolayers and were grown in Dulbecco's modified Eagle medium (DMEM) supplemented with 10% fetal calf serum, penicillin, and streptomycin. The cells were maintained in the calf fetal serum at 37°C in a humidified atmosphere at 5% CO_2. For deep-UV fluorescence imaging studies, the Huh7.5.1 cells were plated in plastic Petri dishes containing 25 mm round quartz coverslip and incubated for 24 hours, leading to deposition of $\sim 240\,000$ cells in each well with quartz slide. Cell attachment was monitored by visible inspection using an optical microscope. After that, the cells were incubated with purified bifunctionalized colloid samples as well as with bare gold nanoparticles and biomolecular solutions. The final concentration of gold in the sample was 10 μM, which corresponds to approximately 10^9 particles per incubated cell, and it was obtained by adding 55 μl of the samples into 3 ml of the medium. In the case of bare gold NPs, due to lower concentration, 150 μl of the colloid was added to 3 ml of medium to ensure the equal final concentration of all the samples. The cell incubation lasted for 6 h. After the incubation, the cells were washed 2 times with PBS and fixed for 1 h with 4% PFA at 4°C. The fixed cells were washed 2 times with distilled water and dried in air.

2.5. Deep-UV fluorescence microscopy

Imaging of the biological samples was carried out on a Zeiss Axioobserver Z-1 microscope (Telemos) at the DISCO beamline of the Synchrotron Soleil, France [50]. Telemos is an epifluorescence microscope, equipped with Zeiss Ultrafluar objective ×40 with a 0.6 numerical aperture that requires glycerine immersion. The microscope uses monochromatic synchrotron radiation as an excitation source in the deep-ultraviolet range between 250 - 350 nm. Fluorescence signals from the samples deposited on quartz coverslips were collected through a set of appropriate filters by PIXIS 1024 BUV camera (Princeton, USA). The whole setup is controlled under μManager [51]. The final resolution of acquired microscopic images was 277 nm with ×40 objective.

DUV imaging for each sample consisted of two sets of experiments: i) steady-state fluorescence imaging of several locations before ii) time-lapse acquisition. We performed the time-lapse experiments on a representative area of the cell culture and acquired fifteen consecutive fluorescence image pairs. The overall acquisition time in the time-lapse experiments was 15 min with constant exposure of the sample to the excitation beam of 290 nm. The selected filters were F1: 355 - 405 nm (Trp emission) and F2: 510 - 560 nm (Rb emission), and acquisition time was 30 s for each image. The images were analyzed using MATLAB software. Only cytoplasmic areas of the cells were considered in this study. Fluorescence signals of each image pixel were corrected by subtracting the background signal and then normalized on their first time-point intensity, before further analysis and comparison of the samples.

3. Results and discussion

3.1. Resonance energy transfer in colloids of gold nanoparticles functionalized by tryptophan and riboflavin

A representative TEM image of Au nanoparticles functionalized by tryptophan and riboflavin (ATR1) is shown in Figure 1. The particles are spherical and the calculated mean diameter is 7.4 ± 1.1 nm. The size distribution follows the lognormal dependence and the fit parameters obtained for the distribution are specified in the right upper corner of the figure. The synthesis procedure of bare gold NPs commonly used in our group results in nearly spherical nanoparticles of ∼8 nm in diameter [29]. The TEM analysis indicates that the functionalization process does not significantly affect the size and morphology of gold nanoparticles. Raman and XPS spectroscopic analyses

were done to confirm the successful functionalization of biomolecules to the nanoparticles (Supplementary Information section 1 and 2), indicating that the molecules are attached to the nanoparticles and in planar orientation with the respect to the surface of the nanoparticles.

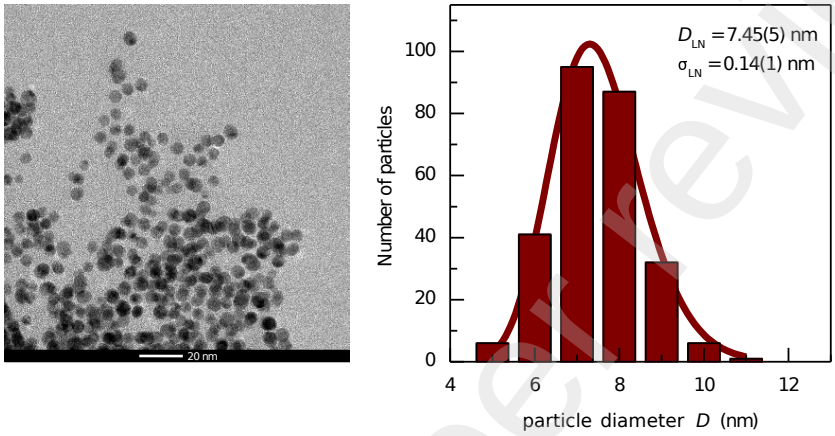

Figure 1: (a) TEM image of gold nanoparticles functionalized by tryptophan and riboflavin biomolecules (ATR1 sample) and (b) the corresponding particle size distribution. The distribution is fitted to lognormal curve with parameters D_{LN} (mode) and σ_{LN} (standard deviation).

UV-vis spectroscopy is used to follow the functionalization of gold nanoparticles. The absorption spectra of bifunctionalized nanoparticles, shown in Figure 2, exhibit features of all three components. The position of the gold surface plasmon resonance peak shifts toward higher wavelengths with an increase in the concentration of riboflavin. This suggests that with an increase in the number of riboflavin molecules in the solution there is an increase in the thickness of the organic layer formed on the surfaces of the nanoparticles. Finally, since the position and the shape of Trp and Rb absorption bands did not change significantly in the presence of gold, the UV-vis spectra imply that the chemical structure of tryptophan and riboflavin molecules is preserved [52]. The UV-vis absorption spectra of the purified functionalized colloids are presented in Figure 2c. The purified samples contain only bounded biomolecules, and their concentration is lower than in as prepared colloids. The characteristic absorption bands of Trp and Rb are clearly observable in the UV-vis spectra of these samples but there is a decrease in their intensity. It has also been noticed that SPR band of gold nanoparticles is red-shifted for about 2 nm confirming the presence of a thin bimolecular layer around

the nanoparticles. The thickness of the organic layer can be estimated by Mie theory [53], taking into account the observed shift and optical constants of gold [54]. Assuming that the diameter of gold nanoparticles is 8 nm, we calculated that the biomolecular layer is ~ 2 nm thick. Finally, the intensity of the absorbance peaks of riboflavin in the spectral range of 350-440 nm is lower in the ATR1 than in the AR1 sample. This suggests that there is a smaller number of riboflavin molecules attached to the NPs in the bifunctionalized nanoparticles, consistent with the additional attachment of tryptophan molecules.

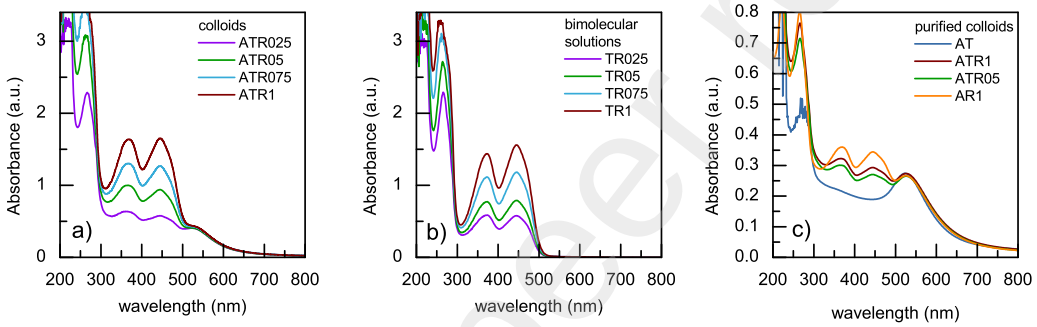

Figure 2: Absorbance spectra for (a) bifunctionalized gold nanoparticles of various riboflavin concentrations, (b) bimolecular solutions of the biomolecules of the corresponding concentration ratios, and (c) selected purified colloids.

The normalized emission and excitation spectra of the aqueous solutions of tryptophan and riboflavin are presented in Figure 3a. It can be seen that the emission band of tryptophan coincides with the low-wavelength excitation peak of riboflavin. Due to this spectral configuration, tryptophan is an efficient donor in the resonance energy transfer (RET) process between Trp and Rb molecules [55].

The RET in the case of bifunctionalized nanoparticles is demonstrated in Figure 3 that shows the photoluminescence (PL) spectra of the bifunctionalized nanoparticle colloids (Figure 3b), the aqueous solutions of tryptophan and riboflavin of the corresponding concentrations (Figure 3c), and the purified colloids (Figure 3d). Apparently, with an increase in the riboflavin concentration, there is a decrease in intensity of the emission band of tryptophan at 360 nm. On the other hand, in the samples with the same concentration of riboflavin, the intensity of the riboflavin fluorescence at 520 nm is higher if tryptophan is present in the system. The observed spectral changes suggest that there

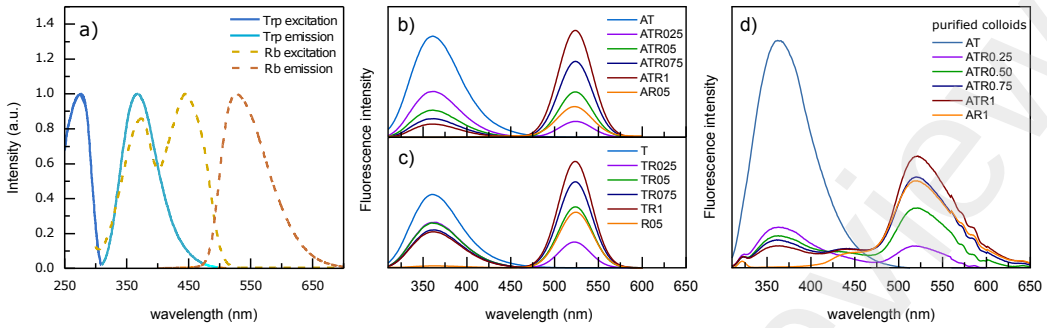

Figure 3: a) Normalized photoluminescence excitation and emission spectra of tryptophan and riboflavin in aqueous solutions. The excitation wavelength was 280/350 nm and the emission wavelength was 300/525 nm for tryptophan and riboflavin solutions respectively. Photoluminescence spectra of (b) gold nanoparticles functionalized by tryptophan and riboflavin, (c) tryptophan and riboflavin mixtures in water, and (d) the purified colloids. In every group (b-d), the riboflavin to gold molar ratio was varied from 0 to 1, with a step of 0.25, whereas the amount of tryptophan is the same in every sample. The excitation wavelength was 290 nm. The concentration of gold was $c_{Au} = 2.5 \times 10^{-6}$ M for the colloids, and $c_{Au} = 27.5 \times 10^{-6}$ M for the purified colloids.

is RET between the molecules in both types of samples (Figure 3b and 3c), but the process appears more pronounced in the case of bifunctionalized nanoparticles (Figure 3b). The RET between Trp and Rb is preserved after the purification process as can be seen in the PL spectra of purified functionalized gold colloids (Figure 3d). The lower intensity of the tryptophan peak in the spectra of the samples that contain riboflavin, compared to the AT sample, suggests that this process takes place between the pairs of biomolecules bound to the nanoparticle surface. This is further confirmed by a comparison of the riboflavin peaks in the spectra of the purified samples ATR1 and AR1 in Figure 3d. As can be seen, riboflavin fluorescence is more pronounced in the sample that contains tryptophan (ATR1). The higher intensity is even more striking as there is less riboflavin adsorbed on the nanoparticles in ATR1 than in the AR1 sample (see Figure 2d). The corresponding PL spectra for these three systems with double concentration of the solutions/colloids are included in Supplementary Information (Figure S4).

As the results above show, both biomolecules retained their fluorescence properties although they are adsorbed on gold nanoparticles. This might be an unexpected effect since the fluorescence of a radiating dipole in contact with a metal surface is usually quenched due to an enhancement in the

nonradiative deexcitation rates. The fluorescence quenching in metal nanoparticle-fluorophores systems could be well described by nanometal surface energy transfer (NSET) theory [56]. For instance, a characteristic distance between the fluorophore and a nearby gold nanoparticle at which the fluorescence of the molecule is quenched by 50% can be calculated as:

$$d_0^{NSET} = (0.225\frac{\Phi_0 c^3}{\omega_{dye}^2 \omega_F k_F})^{\frac{1}{4}}, \quad (1)$$

where c is the speed of light, ω_{mol} is the angular frequency of the emission and Φ_0 is the quantum efficiency of the molecule, while $\omega_F = 8.4 \times 10^{15} rad/s$ and $k_F = 1.2 \times 10^8 cm^{-1}$ are Fermi angular frequency and wavevector for bulk gold [56, 57]. In the case of tryptophan and riboflavin, assuming that their quantum efficiencies are 0.12 and 0.23, the calculated characteristic distances are approximately 4 nm and 6 nm, respectively. The larger distance calculated for Rb is due to the fact that the Rb emission overlaps the SPR of the gold nanoparticles. Both distances are larger than the thickness of the bimolecular layer formed around the nanoparticle, estimated from the SPR shift (Figure 2), implying that the fluorescence of both molecules should be quenched substantially.

Nevertheless, whether the fluorescence of a molecule will be quenched or enhanced in the vicinity of a metal surface depends on many different features of the system under study. This includes the energies of available electronic transitions in the molecules and the metal, the orientation of the molecular dipoles with respect to the metal surface, and, obviously, the distances between the molecules and the surface [41, 57, 58, 38, 59, 60, 61, 62, 63, 64]. Notably, the fluorescence of molecules for which the emission bands coincide with the SPR band of metal is quenched significantly [41, 56, 64, 61, 63]. This is the case for Rb/Au NP in our system, which is why the emission of riboflavin would be expected to be significantly reduced. On the other hand, our Raman spectroscopy results (Supplementary Information section 1) suggest that both molecules are in tangential orientation relative to the Au NP surface. The relative orientation is important because the molecules in tangential orientation are quenched far less than the molecules with dipoles perpendicular to the surface [61]. This could be one of the possible reasons why riboflavin in bifunctionalized Au NP retained its fluorescence. Finally, the intensities of the emission peaks of the biomolecules in the PL spectra are well preserved. Several factors could be responsible for the observed emission behavior; the electromagnetic field might be enhanced in the vicinity of the

metallic particle up to 2.5 times (Supporting Information Figure S5), also, an increase in the radiative rate of the fluorophores can occur when they are positioned at extremely short distances (< 1nm) from the surface of the metal nanoparticles [58, 60].

Resonance energy transfer can be quantified in terms of its efficiency. RET efficiency is commonly defined as $E_{RET} = 1 - F/F_0$ for donor fluorophores, where the intensity of the pure tryptophan emission band is noted as F_0 and the tryptophan band in the presence of riboflavin is represented as F [31, 32, 33]. The efficiency as a function of the acceptor (Rb) concentration is presented in Figure 4. As it can be noticed, the efficiency values for the mixtures of tryptophan and riboflavin biomolecules vary between 0.37 and 0.52, which agrees with the values reported in the literature [55]. On the other hand, in the presence of the nanoparticles, the efficiency coefficients are in the range of 0.54 to 0.87. Since the concentrations of the donor and acceptor molecules in the particular ATRx and TRx samples are the same, the gold nanoparticles increase the efficiency of RET between tryptophan and riboflavin. Also, the values of the F_0/F ratios and the efficiencies are almost independent on the concentration, which, again, suggests a strong influence of the nanoparticles on RET. The estimated RET efficiency for the purified colloids is also included in Figure 4 (depicted in maroon circles). The obtained coefficients fall in the range from 0.82 to 0.90 for both dilutions, suggesting an even more efficient energy transfer between the biomolecules. It is worth noting that the concentration of tryptophan in the purified colloids might not be the same in all of the samples, since the number of Trp molecules in the system cannot be controlled for upon the purification step. This obviously affects the obtained emission spectra and, therefore, the reported efficiencies should be regarded as estimates.

There are several competing processes that occur in the bifunctionalized gold nanoparticles when they are illuminated. The observed enhancement of the RET efficiency between the two molecules in the presence of Au NP might not be a simple sum of these processes [65]. On one hand, the metal influence on adsorbed fluorophores results in a decrease in their photoluminescence and lifetimes, particularly in the case of riboflavin. On the other hand, the fluorophores are brought and kept together on the nanosurface, and in a specific orientation (i.e. tangentially to the surface). The RET efficiency strongly depends on the distance between the donor and acceptor molecules, as well as the mutual orientation of their transition dipoles. Since the molecules attached to the nanoparticles are in close proximity to each other,

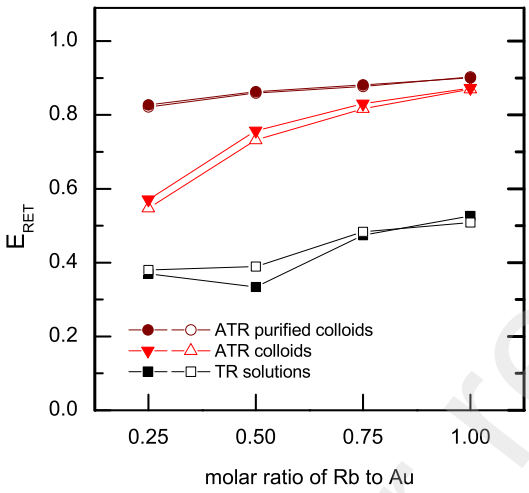

Figure 4: The efficiency of resonant energy transfer between tryptophan and riboflavin molecules when they are immobilized on the surface of gold nanoparticles and when they are free in the solution. The amount of the chemicals used in the samples was calculated with respect to the molar content of the gold nanoparticles. The concentrations of Au nanoparticle were $c_{Au} = 5\,\mu$M (solid symbols) and $c_{Au} = 2.5\,\mu$M (open symbols) in the case of the colloids, while $c_{Au} = 55\,\mu$M (solid symbols) and $c_{Au} = 27.5\,\mu$M (open symbols) for the purified colloids.

it could be expected the efficiency of RET increases. The enhancement of the external EM field in the presence of the metal that is mentioned above may also play its role by affecting the absorbance of the donor molecule [58]. The increase in the probability of Rb excitation due to the appearance of the image dipole of Trp in the vicinity of the gold surface [38] should also be taken into account. However, this effect becomes important when the donor is coupled to the SPR of the nanoparticles and the acceptor molecule is at a distance [41], which is not the case in the present study. Based on the former discussions, we conclude that the observed increase in RET efficiency in these hybrid nanostructures is most probably a consequence of the increased nonradiative deexcitation of riboflavin in the presence of the nanoparticles. Thus, riboflavin has more available electrons in the ground state that could accept the energy transfer from tryptophan. The observed effect might be very important for the design of sensors based on RET molecular systems. By choosing the right type of acceptor molecule-nanoparticle pair, the energy transfer from the donor molecules can be significantly improved. This in turn may enable a substantial increase in the sensitivity of the sensor system.

3.2. DUV fluorescence imaging of human hepatocellular carcinoma cells incubated with functionalized gold nanoparticles

Fluorescence microscopy studies were performed on a human hepatocellular carcinoma-derived Huh7.5 cell line incubated with functionalized gold nanoparticles using DUV synchrotron radiation as an excitation source. Here, we will show that the existence of the resonance energy transfer between tryptophan and riboflavin molecules attached to the gold nanoparticles can help improving the localization of the nanoparticles within the individual cancer cell by fluorescence microscopy. Since the RET induces the changes in photobleaching (PB) dynamics of the biomolecules, the fluorescence that originates from the artificially introduced centers, i.e. AuTrpRb (ATR) nanoparticles, will exhibit different time dependence than the fluorescence that comes from the autofluorophores of the cell. This can be used as an axillary method for resolving the fluorescence signal that comes from the nanoparticles utilizing fluorescence imaging.

The influence of RET on the donor photobleaching dynamics is schematically presented in Figure 5. As a consequence of RET, the fluorescence lifetime of the donor (tryptophan) molecule shortens [66], leading to a reduction of its PB in the spectral range of the donor fluorescence [67, 68, 48]. On the other hand, even though the lifetime of the acceptor's excited state is not influenced by RET [66], the degree of photobleaching of the acceptor molecule in the RET pair scales with the RET efficiency [69], probably due to a change in the population of the acceptor's excited states. In the previous section, it is shown that gold nanoparticles promote the RET between tryptophan and riboflavin. Consequently, the change in the PB rates of the molecules would be more pronounced in the presence of the nanoparticles. The photobleaching would decrease for the donor and increase for the acceptor molecules, compared to the RET pair that is not influenced by the particle surface.

The PB dynamic of Huh7.5 cells incubated by functionalized gold nanoparticles of different compositions was studied by DUV time-lapse fluorescence microscopy in the F1 [355 - 405 nm] and F2 [510 - 560 nm] spectral ranges, as it is described in Section 2.5. These spectral ranges correspond to tryptophan (F1) and riboflavin (F2) emission ranges. Typical images of the Huh-ATR1 sample obtained by using this procedure are given in Figure 6. Bright-field images (Supplementary Information Figure S6) showed that the cells preserved their characteristic triangular shape after the incubation, with a distinctive and intact nucleus. This suggested that the gold nanoparticles

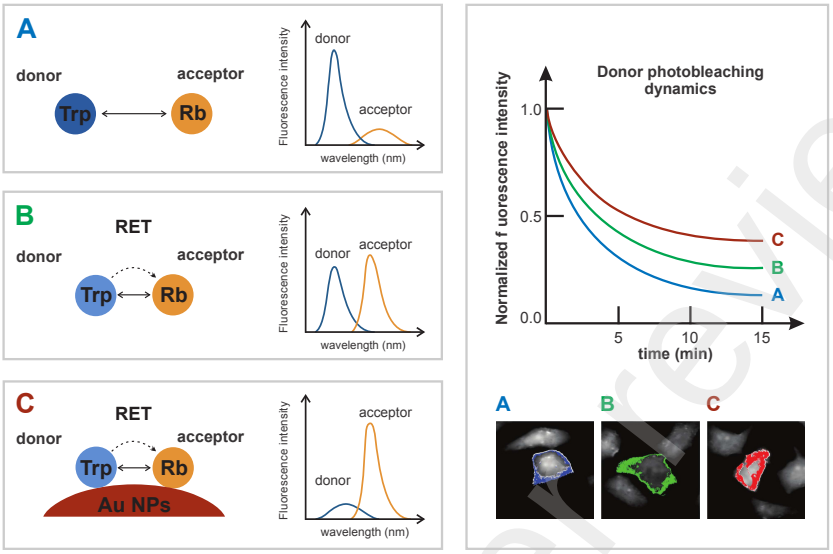

Figure 5: The effects of RET on the donor photobleaching dynamics. Different surroundings the donor molecules (A: acceptor molecules are far away from the donor molecules; B: acceptor molecules are close to the donor molecules; C: both donor and acceptor molecules are adsorbed on gold nanoparticles) influence the donor fluorescence intensity, which is reflected on the donor photobleaching dynamics (upper right graph). The fact that the same molecules will exhibit different photobleaching behavior depending on their environment can be consequently employed in the time-lapse bioimaging study of human cancer cells in order to localize the functionalized gold nanoparticles after the incubation (lower right microscopy images). Abbreviations: Trp - tryptophan; Rb - riboflavin; Au NPs - gold nanoparticles

(at the low concentration used here) are not cytotoxic for human cell lines, which is in agreement with other studies [70, 71, 72, 73, 74, 75, 76, 77]. The non-toxicity is also confirmed by the steady-state fluorescence images, shown in Figure S7 in Supplementary Information, for the control, Huh-A, Huh-AT and Huh ATR1 samples acquired in both spectral ranges.

The uptake of nanostructured gold particles by the carcinoma cells is well documented in the literature [78, 79, 73, 80, 75, 81]. However, very few studies report the internalization of the nanoparticles in the cell nucleus [82, 83]. For example, Nativo *et al.* [83] observed the presence of gold nanoparticles in the nuclei of HeLa cells, but only for the nanoparticles functionalized with cell-penetrating peptides for nucleus labeling. In the present study, the treatment with bifunctionalized nanoparticles did not induce observable changes in the nucleus fluorescence. For this reason, we excluded the nucleus

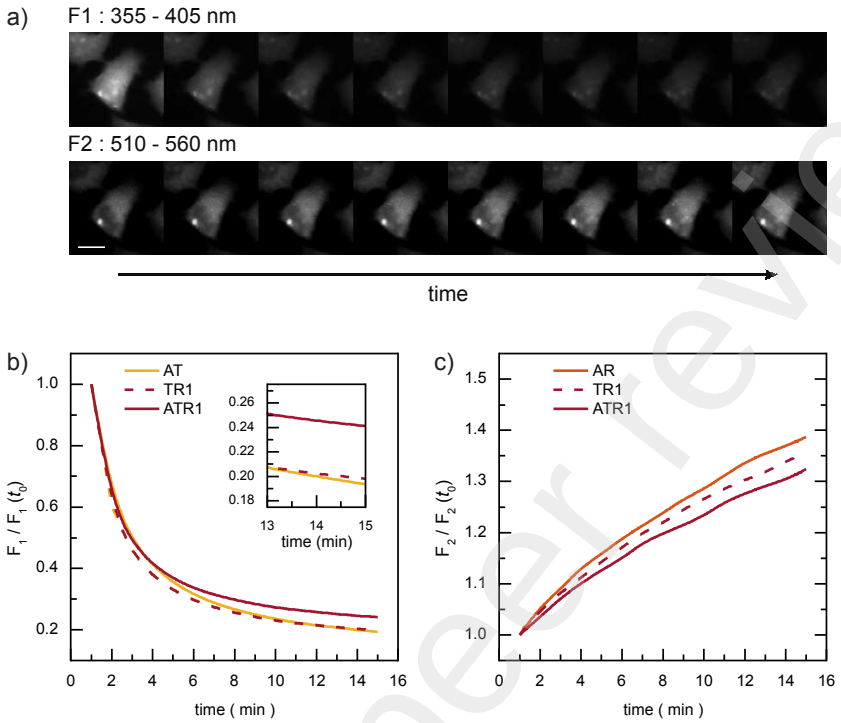

Figure 6: (a) Fluorescence time-lapse images of bifunctionalized gold nanoparticles (ATR1) treated Huh7.5.1 cells human liver cancer cells acquired in F1 [355 - 405 nm] and F2 [510 - 560 nm] spectral ranges (upper and lower image sequence, respectively), with an arrow depicting the time evolution of the signal. Scale bar is 30 μm, and the excitation wavelength was 290 nm. (b) Time dependence of the normalized fluorescence intensities averaged over the cytoplasmic region of Huh 7.5.1 cells treated with tryptophan functionalized gold (AT), tryptophan-riboflavin (TR1) solutions and bifunctionalized gold (ATR1) colloids in F1 spectral range [355 - 405 nm]. The inset shows the last three time points of the fluorescence intensities in the F1 range. (c) Time dependence of the normalized fluorescence intensities averaged over the cytoplasmic region of Huh 7.5.1 cells treated with riboflavin functionalized gold (AR), tryptophan-riboflavin (TR1) solutions and bifunctionalized gold (ATR1) colloids in F2 spectral range [510 - 560 nm].

region from our analyses. The segmentation was made manually for each sample and the average values of the intensity of the fluorescence signal were calculated over the selected region for every image. The time-dependences of the average fluorescence intensities for cancer liver cells incubated with tryptophan-functionalized gold nanoparticles (AT), riboflavin-functionalized gold nanoparticles (AR), tryptophan-riboflavin solution (TR1) and bifunctionalized gold nanoparticles (ATR1) in the spectral windows F1 and F2 are shown in

Figure 6b and 6c. Note that both the fluorescence from the autofluorophores and the (bi)functionalized nanoparticles contribute to the values of the average fluorescence intensity.

The time dependences of the average fluorescence intensities in the F1 window ($F_1(t)$), presented in Figure 6b, show that every sample exhibits typical photobleaching in this spectral range [24]. Also, it can be seen that the rate of the PB processes varies between the samples, which results in different values of the saturation intensity at the end of the process $F_{1,sat} = F_1(t = t_{max})$. The inset to Figure 6b shows the comparison between the saturation intensities of the treated Huh cells samples. The difference in the $F_{1,sat}$ values between the Huh-ATR1 and Huh-AT samples is about 5%, which is remarkable considering that the intensities are averaged over the whole cytoplasmic region. The higher the saturation values are, the lower are the decay rates of the photoluminescence signal via photobleaching (PB rates). Therefore, the higher PB saturation value of the Huh-ATR1 sample indicates that new pathways for the nonradiative deexcitation of tryptophan are formed after the cofunctionalization of the nanoparticles with riboflavin. This effect can be attributed to the RET between tryptophan and riboflavin molecules adsorbed on the Au NP.

In the F2 range the fluorescence signals increase over time, as shown in Figure 6c. This behavior corresponds to the general evolution of the autofluorescence upon interaction of biological material with UV radiation, which results in generation of new fluorophores in the processes of photoconversion that emit in this range [24, 84]. Figure 6c also shows that there is a difference in the rates of fluorescence increase depending on the cell treatment. This indicates that in addition to the photogeneration of the autofluorescence, the photobleaching of the fluorophores manifests differently, depending on the sample [25]. The signal from the cells incubated with both tryptophan and riboflavin increases more slowly over time than the signal coming from the cells incubated with just one type of the molecule. This effect is even more pronounced in the presence of gold nanoparticles. The slower increase in the fluorescence intensity observed for the Huh-ATR1 sample compared to that of the Huh-TR1 sample is a consequence of an increased PB rate due to higher RET efficiency of functionalized gold nanoparticles (Figure 5). More specifically, when the biomolecules are close to each other, tryptophan induces an increase in the population of the excited states of riboflavin that results in its stronger photobleaching [69], observable in the F2 range. The results presented in Figure 6b and 6c clearly show that the dependence

of normalized averaged signals on time is affected by the cell treatment. The time-lapse measurements were also performed on the cells treated with all of the colloids/solutions used in the present study. The normalized evolutions of the fluorescence of all colloid-treated Huh cells were included in the Supplementary Information (Figure S8 and S9).

The analysis of the photobleaching dynamics of the samples suggested that there is a possibility of separation of areas in the cells of different compositions. To do this, we followed the evolution of the fluorescence for every pixel in the cells (except those in the nuclei) and classified them according to their saturation values. Like most radiation processes, photobleaching can be described by exponential time-dependence [85]. Faster photobleaching results in lower relative saturation values of the signal, which we used as a classification marker.

Typical results obtained by the pixel categorization procedure for the Huh control, Huh-A, Huh-AT, Huh-AR and Huh-ATR1 samples are shown in Figure 7 a and b for the F1 (with intervals of 0.05) and the F2 (with intervals of 0.1) range, respectively. The figures show the images of the samples with the corresponding pixel masks marked in green. The masks depict the areas of different photobleaching dynamics, corresponding to different ranges of saturation values. Overall, the spatial distribution of the pixels from the particular category varies from sample to sample, which implies the presence of additional fluorophores of exogenous origin and justifies the classification approach. Regardless of the sample in the F1 range (Figure 7a), a negligible number of pixels exhibited a saturation value below 15% of the initial signal and that value imposed the lower limit for the categorization. The pixels with saturation values higher than 0.45 in the F1 range cover regions close to the cell edges. Similarly, the cell edges can be classified into the 1.0-1.1 category in the F2 spectral window (Figure 7b). These two categories correspond to the smallest changes in fluorescence intensity over time and can be attributed to a lack of the cell material (since the thickness of the cell decreases outwards its center).

A comparison of the samples reveals an apparent influence of the functionalized nanoparticles on the PB dynamics of Huh cells. In the F1 range (Figure 7a), the photobleaching of the cells incubated with the nanoparticles is obviously more pronounced, since a higher number of pixels belong to the lower categories. On the other hand, in the F2 range (Figure 7b) the incubated cells show a large number of pixels in the categories 1.1-1.2 and 1.2-1.3, which cover areas in the interior of the cells. The complete distribution

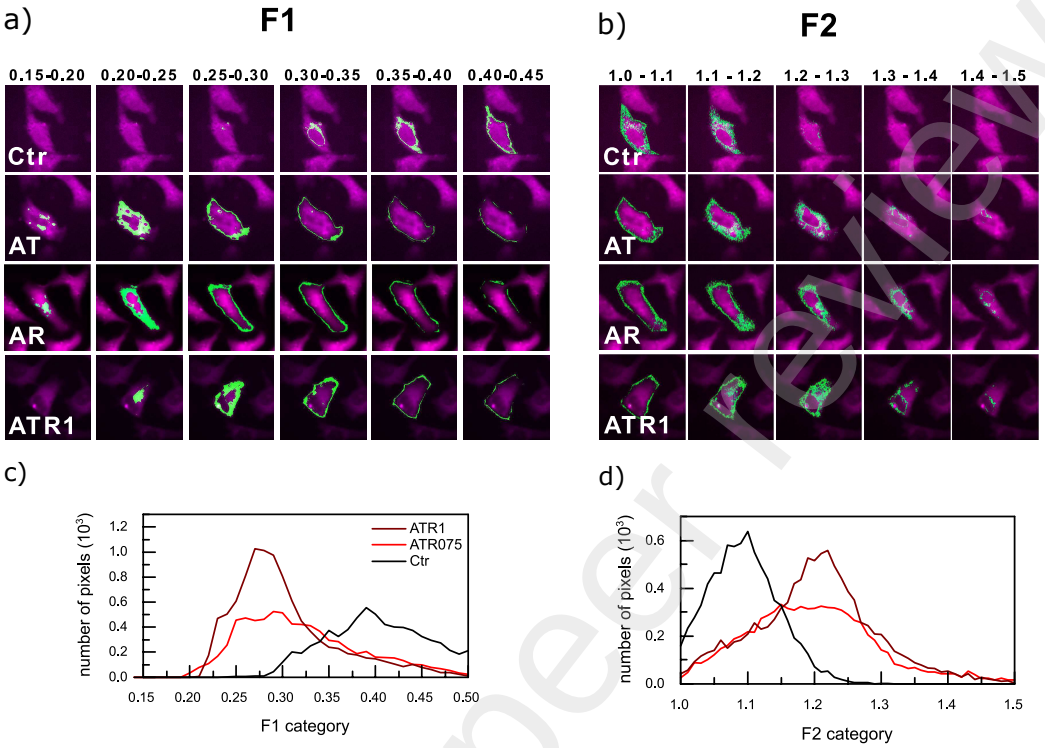

Figure 7: Visual representation of the procedure for the pixel categorization in a) F1 [355 - 405 nm] and b) F2 [510 - 560 nm] spectral ranges. The categorization was based on ratios of the signal intensity at the end of the time-lapse measurement and the initial signal intensity of each pixel. In the images of Huh control (1st row), Huh-AT (2nd row), Huh-AR (3rd row) and Huh-ATR1 (4th row) samples, the pixels that belong to particular categories (columns) were presented as green areas. (c) The distribution of the saturation values of the fluorescence intensity for the Huh-ATR1 (maroon), Huh-ATR075 (red) and Huh control (black) samples over various F1 categories. (d) The distribution of the saturation values of fluorescence intensity for same set of the samples over F2 categories.

of the saturation values in both spectral ranges is given in the Supplementary Information (Figure S10 and S11), whereas the temporal $F_2(t)=f(F_1(t))$ curves are shown in Figure S12. The comparison of the distributions calculated for the Huh-ATR1, Huh-ATR075, and the control samples is given in Figure 7c and 7d. It can be seen that in the case of gold nanoparticles functionalized by both biomolecules, the largest number of pixels falls into the 0.25-0.30 category for the F1 range and around 1.25 for the F2. The observed distribution of the saturation values is in stark contrast to the control, but also different from the observed distribution for the sample containing Au NP functionalized

by single molecules (Trp or Rb).

The pixel classification procedure explained above enables discrimination of the intrinsic from the extrinsic fluorescence centers and the main results are presented in Figure 8. In the fluorescence images of the control, Huh-ATR075, and Huh-ATR1 samples, we highlighted the pixels from two specific categories acquired by the classification: 0.25 - 0.30 for the F1 range (second column) and 1.10 - 1.20 for the F2 range (third column). Figure 8 also shows the overlap between these two sets of pixels, marked on both the fluorescence (the fourth column) and the bright-field (the fifth column) images. As it can be seen, the images of the samples incubated with the nanoparticles are different from that of the control sample. In the image of the control sample, very few pixels belong to the 0.25 - 0.30 category of F1 leading to negligible overlap between the channels. The control sample does possess pixels that belong to the 1.1 - 1.2 category of F2 because of, as previously discussed, the photogeneration of fluorophores. On the other hand, in the images of the cells incubated with ATR075 and ATR1 colloids, the overlap of the two masks covers a wider area of the cells. These areas, as it can be noticed in the bright-field images, are rich in biological material. The observed pixels represent fluorophores that exhibit PB behavior consistent with PB dynamics of the tryptophan-riboflavin RET pair at the surface of gold nanoparticles, which implies that the suggested procedure can be used to identify the regions where the nanoparticles accumulate within the cell.

4. Conclusion

Adsorption of tryptophan (donor) and riboflavin (acceptor) onto gold nanoparticles can strongly affect resonance energy transfer between these two biomolecules. Although the surface plasmon resonance of gold nanoparticles coincides with the emission peak of riboflavin, only a moderate quenching of the fluorescence is observed. In contrast, the efficiency of the RET process in the bifunctionalized nanoparticles was substantially higher than in the case of the aqueous mixture of the biomolecules. The increase in the RET efficiency was attributed to an increase in nonradiative deexcitation of riboflavin in the presence of gold surface, which facilitated the energy transfer from tryptophan. Next, the photobleaching dynamics of hepatocellular carcinoma cells incubated with tryptophan and riboflavin functionalized gold nanoparticles was investigated by time-lapse synchrotron radiation DUV fluorescence microscopy. The treatment of the Huh7.5.1 cells with bifunctionalized nanoparticles introduces new fluorescence

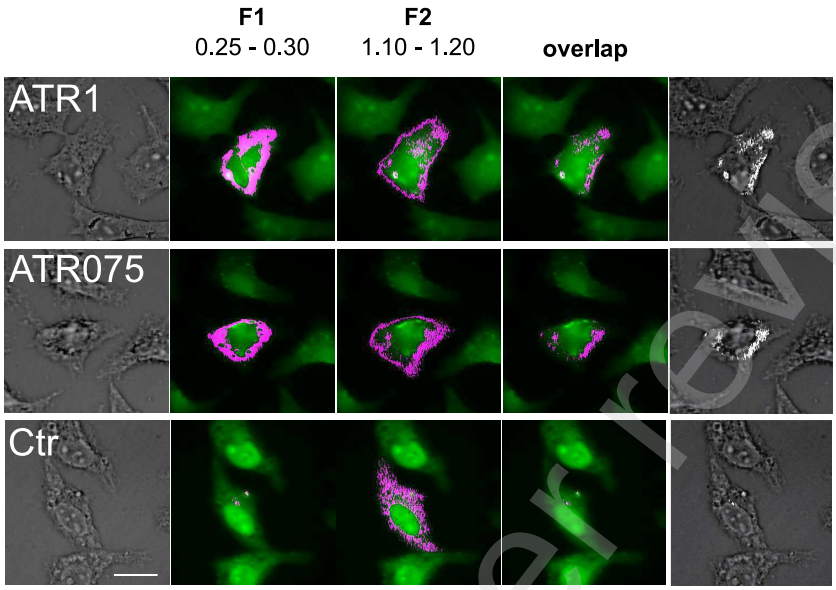

Figure 8: (a) Visible and fluorescence (F1 spectral range) images of Huh-ATR1 (first row), Huh-ATR075 (second row) and Huh-Ctr (third row) samples. The images in the second and third columns were overlaid with the category masks (0.20 - 0.30 category from F1 range and 1.10 - 1.20 category from F2 range). The overlaps of the second and third columns images depict the pixels that belong to both categories and show the most probable sites of the functionalized gold nanoparticles. The overlaps are presented in the fluorescence (fourth column) and the visible images (fifth column). Scale bar is 30 μm

centers. The photobleaching dynamics of these centers is different from that of the autofluorophores of the cell itself. For this reason, we introduced the classification of pixels in fluorescence images that is based on the differences in the photobleaching dynamics of the fluorescence centers depending on their origin. The presented approach opened a possibility for indirect optical localization of biomolecule-functionalized metal nanoparticles in complex biological material using conventional fluorescence microscopy techniques, even if the particles were smaller than the lateral resolution of the fluorescence image. It is important to note that these results suggest that the metal nanoparticles can be used in order to improve the sensitivity of the RET-based sensors. Also, an increase in RET efficiency in the presence of the nanoparticle means that some other naturally occurring fluorophores can be employed in the preparation of the sensors, which are sometimes neglected due to their low signaling power.

Acknowledgements

J. P. is thankful to Dr. Julia Vergalli for her help and valuable support, and to Dr. Frederic Jamme for fruitful discussions on imaging procedures. We acknowledge SOLEIL for provision of synchrotron radiation facilities and we would like to thank Valerie Rouam for assistance in using beamline DISCO. The authors kindly acknowledge also the help of Blandine Pineau for the technical assistance.

Deep UV imaging of the incubated cells was performed at the DISCO beamline of Synchrotron Soleil (France) within the scope of the project No. 20131218. This work is funded by Ministry of Science, Technological development and Innovations of the Republic of Serbia (Grants: 451-03-47/2023-01/200017 and 451-03-47/2023-01/200162).

References

[1] J. Ma, X. Wang, J. Feng, C. Huang, Z. Fan, Individual plasmonic nanoprobes for biosensing and bioimaging: recent advances and perspectives, Small 17 (8) (2021) 2004287.

[2] M. A. Dheyab, A. A. Aziz, P. Moradi Khaniabadi, M. S. Jameel, N. Oladzadabbasabadi, S. A. Mohammed, R. S. Abdullah, B. Mehrdel, Monodisperse gold nanoparticles: A review on synthesis and their application in modern medicine, International Journal of Molecular Sciences 23 (13) (2022) 7400.

[3] S. J. Amina, B. Guo, A review on the synthesis and functionalization of gold nanoparticles as a drug delivery vehicle, International journal of nanomedicine 15 (2020) 9823.

[4] N. Elahi, M. Kamali, M. H. Baghersad, Recent biomedical applications of gold nanoparticles: A review, Talanta 184 (2018) 537–556.

[5] J. R. Navarro, F. Lerouge, From gold nanoparticles to luminescent nano-objects: experimental aspects for better gold-chromophore interactions, Nanophotonics 6 (1) (2017) 71–92.

[6] K. Saha, S. S. Agasti, C. Kim, X. Li, V. M. Rotello, Gold nanoparticles in chemical and biological sensing, Chem. Rev. 112 (5) (2012) 2739–2779.

[7] A. M. Alkilany, C. J. Murphy, Toxicity and cellular uptake of gold nanoparticles: What we have learned so far?, J. Nanopart. Res. 12 (7) (2010) 2313–2333.

[8] V. Amendola, R. Pilot, M. Frasconi, O. M. Maragò, M. A. Iatì, Surface plasmon resonance in gold nanoparticles: a review, Journal of Physics: Condensed Matter 29 (20) (2017) 203002.

[9] J. W. Lee, S.-R. Choi, J. H. Heo, Simultaneous stabilization and functionalization of gold nanoparticles via biomolecule conjugation: Progress and perspectives, ACS Applied Materials & Interfaces 13 (36) (2021) 42311–42328.

[10] F. Dumur, E. Dumas, C. R. Mayer, Functionalization of gold nanoparticles by inorganic entities, Nanomaterials 10 (3) (2020) 548.

[11] E. A. Barnoy, M. Motiei, C. Tzror, S. Rahimipour, R. Popovtzer, D. Fixler, Biological logic gate using gold nanoparticles and fluorescence lifetime imaging microscopy, ACS Applied Nano Materials 2 (10) (2019) 6527–6536.

[12] J. Langer, S. M. Novikov, L. M. Liz-Marzán, Sensing using plasmonic nanostructures and nanoparticles, Nanotechnology 26 (32) (2015) 322001.

[13] O. S. Wolfbeis, An overview of nanoparticles commonly used in fluorescent bioimaging, Chem. Soc. Rev. 44 (14) (2015) 4743–4768.

[14] C. Lai-Kwan, H.-T. Chang, From Bioimaging to Biosensors: Noble Metal Nanoparticles in Biodetection, Pan Stanford, 2012.

[15] W. Yang, B. Xia, L. Wang, S. Ma, H. Liang, D. Wang, J. Huang, Shape effects of gold nanoparticles in photothermal cancer therapy, Materials Today Sustainability 13 (2021) 100078.

[16] A. Alhussan, E. P. D. Bozdoğan, D. B. Chithrani, Combining gold nanoparticles with other radiosensitizing agents for unlocking the full potential of cancer radiotherapy, Pharmaceutics 13 (4) (2021) 442.

[17] I. Maliszewska, E. Wanarska, A. C. Thompson, I. D. Samuel, K. Matczyszyn, Biogenic gold nanoparticles decrease methylene blue

photobleaching and enhance antimicrobial photodynamic therapy, Molecules 26 (3) (2021) 623.

[18] A. Bucharskaya, G. Maslyakova, G. Terentyuk, A. Yakunin, Y. Avetisyan, O. Bibikova, E. Tuchina, B. Khlebtsov, N. Khlebtsov, V. Tuchin, Towards effective photothermal/photodynamic treatment using plasmonic gold nanoparticles, International journal of molecular sciences 17 (8) (2016) 1295.

[19] K. He, T. Shokuhfar, R. Shahbazian-Yassar, Imaging of soft materials using in situ liquid-cell transmission electron microscopy, Journal of Physics: Condensed Matter 31 (10) (2019) 103001.

[20] J. Vergalli, E. Dumont, J. Pajović, B. Cinquin, L. Maigre, M. Masi, M. Refregiers, J.-M. Pages, Spectrofluorimetric quantification of antibiotic drug concentration in bacterial cells for the characterization of translocation across bacterial membranes, Nat. Protoc. 13 (6) (2018) 1348.

[21] J. Vergalli, E. Dumont, B. Cinquin, L. Maigre, J. Pajović, E. Bacqué, M. Mourez, M. Réfrégiers, J.-M. Pagès, Fluoroquinolone structure and translocation flux across bacterial membrane, Sci. Rep. 7 (1) (2017) 9821.

[22] A. Allam, L. Maigre, J. Vergalli, E. Dumont, B. Cinquin, R. A. de Sousa, J. Pajović, E. Pinet, N. Smith, J.-P. Herbeuval, et al., Microspectrofluorimetry to dissect the permeation of ceftazidime in gram-negative bacteria, Sci. Rep. 7 (1) (2017) 986.

[23] S. Kaščáková, L. Maigre, J. Chevalier, M. Réfrégiers, J.-M. Pages, Antibiotic transport in resistant bacteria: Synchrotron UV fluorescence microscopy to determine antibiotic accumulation with single cell resolution, PLoS One 7 (6) (2012) e38624.

[24] B. Cinquin, L. Maigre, E. Pinet, J. Chevalier, R. A. Stavenger, S. Mills, M. Réfrégiers, J.-M. Pagès, Microspectrometric insights on the uptake of antibiotics at the single bacterial cell level, Sci. Rep. 5 (2015) 17968.

[25] R. Dojčilović, J. D. Pajović, D. K. Božanić, N. Jović, V. P. Pavlović, V. B. Pavlović, L. Lenhardt Acković, I. Zeković, M. Dramićanin,

S. Kaščaková, M. Réfrégiers, G. Rašić, B. Vlahović, V. Djoković, DUV fluorescence bioimaging study of the interaction of partially reduced graphene oxide and liver cancer cells, 2D Mater. 5 (4) (2018) 045019.

[26] R. Dojčilović, J. D. Pajović, D. K. Božanić, U. Bogdanović, V. V. Vodnik, S. Dimitrijević-Branković, M. G. Miljković, S. Kaščaková, M. Réfrégiers, V. Djoković, Interaction of amino acid-functionalized silver nanoparticles and candida albicans polymorphs: A deep-UV fluorescence imaging study, Colloids Surf., B 155 (2017) 341–348.

[27] R. Dojčilović, J. D. Pajović, D. K. Božanić, V. V. Vodnik, S. Dimitrijević-Branković, A. R. Milosavljević, S. Kaščàkovà, M. Réfrégiers, V. Djoković, A fluorescent nanoprobe for single bacterium tracking: Functionalization of silver nanoparticles with tryptophan to probe the nanoparticle accumulation with single cell resolution, Analyst 141 (6) (2016) 1988–1996.

[28] J. D. Pajović, R. Dojčilović, D. K. Božanić, V. V. Vodnik, S. Dimitrijević-Branković, S. Kaščaková, M. Réfrégiers, M. Markelić, V. Djoković, Deep UV ffluorescence imaging study of Candida albicans cells treated with gold-riboflavin hydrocolloids, Opt. Quantum Electron. 48 (6) (2016) 311.

[29] J. D. Pajović, R. Dojčilović, D. K. Božanić, S. Kaščáková, M. Réfrégiers, S. Dimitrijević-Branković, V. V. Vodnik, A. R. Milosavljević, E. Piscopiello, A. S. Luyt, et al., Tryptophan-functionalized gold nanoparticles for deep UV imaging of microbial cells, Colloids Surf., B 135 (2015) 742–750.

[30] J. S. Lindsey, M. Taniguchi, D. F. Bocian, D. Holten, The fluorescence quantum yield parameter in Förster resonance energy transfer (FRET)—meaning, misperception, and molecular design, Chemical Physics Reviews 2 (1) (2021) 011302.

[31] B. Valeur, M. N. Berberan-Santos, Molecular Fluorescence: Principles and Applications, John Wiley & Sons, 2012.

[32] P. J. Walla, Modern Biophysical Chemistry: Detection and Analysis of Biomolecules, John Wiley & Sons, 2014.

[33] A. Govorov, P. L. H. Martínez, H. V. Demir, Understanding and Modeling Förster-type Resonance Energy Transfer (FRET): Introduction to FRET, Vol. 1, Springer, 2016.

[34] H. Zong, X. Wang, X. Mu, J. Wang, M. Sun, Plasmon-enhanced fluorescence resonance energy transfer, The Chemical Record 19 (5) (2019) 818–842.

[35] T. Ozel, P. L. Hernandez-Martinez, E. Mutlugun, O. Akin, S. Nizamoglu, I. O. Ozel, Q. Zhang, Q. Xiong, H. V. Demir, Observation of selective plasmon-exciton coupling in nonradiative energy transfer: Donor-selective versus acceptor-selective plexcitons, Nano Lett. 13 (7) (2013) 3065–3072.

[36] L. Zhao, T. Ming, L. Shao, H. Chen, J. Wang, Plasmon-controlled förster resonance energy transfer, J. Phys. Chem. C 116 (14) (2012) 8287–8296.

[37] J. I. Gersten, A. Nitzan, Accelerated energy transfer between molecules near a solid particle, Chem. Phys. Lett. 104 (1) (1984) 31–37.

[38] X. Hua, J. Gersten, A. Nitzan, Theory of energy transfer between molecules near solid state particles, J. Chem. Phys. 83 (7) (1985) 3650–3659.

[39] J. Zhang, Y. Fu, J. R. Lakowicz, Enhanced förster resonance energy transfer (FRET) on a single metal particle, J. Phys. Chem. C 111 (1) (2007) 50–56.

[40] J. Zhang, Y. Fu, M. H. Chowdhury, J. R. Lakowicz, Enhanced förster resonance energy transfer on single metal particle. 2. dependence on donor-acceptor separation distance, particle size, and distance from metal surface, J. Phys. Chem. C 111 (32) (2007) 11784–11792.

[41] C. A. Marocico, X. Zhang, A. L. Bradley, A theoretical investigation of the influence of gold nanosphere size on the decay and energy transfer rates and efficiencies of quantum emitters, J. Chem. Phys. 144 (2) (2016) 024108.

[42] C. D. Geddes, Metal-Enhanced Fluorescence, John Wiley & Sons, 2010.

[43] B. Foerster, V. A. Spata, E. A. Carter, C. Sönnichsen, S. Link, Plasmon damping depends on the chemical nature of the nanoparticle interface, Science advances 5 (3) (2019) eaav0704.

[44] W. Ding, L.-Y. Hsu, G. C. Schatz, Plasmon-coupled resonance energy transfer: A real-time electrodynamics approach, The Journal of Chemical Physics 146 (6) (2017) 064109.

[45] L.-Y. Hsu, W. Ding, G. C. Schatz, Plasmon-coupled resonance energy transfer, The Journal of Physical Chemistry Letters 8 (10) (2017) 2357–2367.

[46] J. Bohlen, Á. Cuartero-González, E. Pibiri, D. Ruhlandt, A. Fernández-Domínguez, P. Tinnefeld, G. P. Acuna, Plasmon-assisted Förster resonance energy transfer at the single-molecule level in the moderate quenching regime, Nanoscale 11 (16) (2019) 7674–7681.

[47] H. Li, Y. Zhao, Z. Chen, D. Xu, Silver enhanced ratiometric nanosensor based on two adjustable fluorescence resonance energy transfer modes for quantitative protein sensing, Biosensors and Bioelectronics 87 (2017) 428–432.

[48] A. Pietraszewska-Bogiel, T. Gadella, Fret microscopy: from principle to routine technology in cell biology, Journal of microscopy 241 (2) (2011) 111–118.

[49] S. J. Sahl, S. W. Hell, S. Jakobs, Fluorescence nanoscopy in cell biology, Nat. Rev. Mol. Cell Biol. 18 (11) (2017) 685.

[50] F. Jamme, S. Kaščaková, S. Villette, F. Allouche, S. Pallu, V. Rouam, M. Réfrégiers, Deep UV autofluorescence microscopy for cell biology and tissue histology, Biol. Cell 105 (7) (2013) 277–288.

[51] A. Edelstein, N. Amodaj, K. Hoover, R. Vale, N. Stuurman, Computer control of microscopes using μmanager, Curr. Protoc. Mol. Biol. 92 (1) (2010) 14–20.

[52] M. C. Vallette, A. Edwards, S. Kennedy, E. Silva, J. Derouault, M. Rey-Lafon, et al., Photo-induced generation of the riboflavin-tryptophan adduct and a vibrational interpretation of its structure, Vibrational spectroscopy 6 (2) (1994) 173–183.

[53] W. Hergert, T. Wriedt, The Mie theory: basics and applications, Vol. 169, Springer, 2012.

[54] P. B. Johnson, R.-W. Christy, Optical constants of the noble metals, Physical review B 6 (12) (1972) 4370.

[55] P. Li, S. Liu, X. Wang, Z. Liu, Y. He, Fluorescence quenching studies on the interaction of riboflavin with tryptophan and its analytical application, Luminescence 28 (6) (2013) 910–914.

[56] M. P. Singh, G. F. Strouse, Involvement of the lspr spectral overlap for energy transfer between a dye and au nanoparticle, Journal of the American Chemical Society 132 (27) (2010) 9383–9391.

[57] T. Jennings, M. Singh, G. Strouse, Fluorescent lifetime quenching near d= 1.5 nm gold nanoparticles: probing nset validity, Journal of the American Chemical Society 128 (16) (2006) 5462–5467.

[58] H. Mishra, B. L. Mali, J. Karolin, A. I. Dragan, C. D. Geddes, Experimental and theoretical study of the distance dependence of metal-enhanced fluorescence, phosphorescence and delayed fluorescence in a single system, Physical Chemistry Chemical Physics 15 (45) (2013) 19538–19544.

[59] M. Swierczewska, S. Lee, X. Chen, The design and application of fluorophore–gold nanoparticle activatable probes, Physical Chemistry Chemical Physics 13 (21) (2011) 9929–9941.

[60] E. Dulkeith, A. C. Morteani, T. Niedereichholz, T. A. Klar, J. Feldmann, S. A. Levi, F. C. van Veggel, D. N. Reinhoudt, M. Möller, D. I. Gittins, Fluorescence quenching of dye molecules near gold nanoparticles: radiative and nonradiative effects, Physical review letters 89 (20) (2002) 203002.

[61] P. Reineck, D. Gómez, S. H. Ng, M. Karg, T. Bell, P. Mulvaney, U. Bach, Distance and wavelength dependent quenching of molecular fluorescence by au@ sio2 core–shell nanoparticles, ACS nano 7 (8) (2013) 6636–6648.

[62] R. Chhabra, J. Sharma, H. Wang, S. Zou, S. Lin, H. Yan, S. Lindsay, Y. Liu, Distance-dependent interactions between gold nanoparticles

and fluorescent molecules with *dna* as tunable spacers, Nanotechnology 20 (48) (2009) 485201.

[63] X. Zhang, C. A. Marocico, M. Lunz, V. A. Gerard, Y. K. Gun'Ko, V. Lesnyak, N. Gaponik, A. S. Susha, A. L. Rogach, A. L. Bradley, Wavelength, concentration, and distance dependence of nonradiative energy transfer to a plane of gold nanoparticles, ACS nano 6 (10) (2012) 9283–9290.

[64] Y. Chen, K. Munechika, D. S. Ginger, Dependence of fluorescence intensity on the spectral overlap between fluorophores and plasmon resonant single silver nanoparticles, Nano letters 7 (3) (2007) 690–696.

[65] N. Aissaoui, K. Moth-Poulsen, M. Käll, P. Johansson, L. M. Wilhelmsson, B. Albinsson, Fret enhancement close to gold nanoparticles positioned in dna origami constructs, Nanoscale 9 (2) (2017) 673–683.

[66] M. Y. Berezin, S. Achilefu, Fluorescence lifetime measurements and biological imaging, Chemical reviews 110 (5) (2010) 2641–2684.

[67] P. J. Verveer, Advanced Fluorescence Microscopy: Methods and Protocols, Springer, 2015.

[68] Y. Sun, R. N. Day, A. Periasamy, Investigating protein-protein interactions in living cells using fluorescence lifetime imaging microscopy, Nat. Protoc. 6 (9) (2011) 1324.

[69] X. Kong, E. Nir, K. Hamadani, S. Weiss, Photobleaching pathways in single-molecule FRET experiments, Journal of the American Chemical Society 129 (15) (2007) 4643–4654.

[70] P. Ghosh, X. Yang, R. Arvizo, Z.-J. Zhu, S. S. Agasti, Z. Mo, V. M. Rotello, Intracellular delivery of a membrane-impermeable enzyme in active form using functionalized gold nanoparticles, J. Am. Chem. Soc. 132 (8) (2010) 2642–2645.

[71] S. Parveen, R. Misra, S. K. Sahoo, Nanoparticles: a boon to drug delivery, therapeutics, diagnostics and imaging, Nanomedicine: NBM 8 (2) (2012) 147 – 166.

[72] K. McNamara, S. A. Tofail, Nanoparticles in biomedical applications, Adv. Phys.: X 2 (1) (2017) 54–88.

[73] B. Duncan, C. Kim, V. M. Rotello, Gold nanoparticle platforms as drug and biomacromolecule delivery systems, J. Controlled Release 148 (1) (2010) 122–127.

[74] S. Rana, A. Bajaj, R. Mout, V. M. Rotello, Monolayer coated gold nanoparticles for delivery applications, Adv. Drug Delivery Rev. 64 (2) (2012) 200–216.

[75] E. E. Connor, J. Mwamuka, A. Gole, C. J. Murphy, M. D. Wyatt, Gold nanoparticles are taken up by human cells but do not cause acute cytotoxicity, Small 1 (3) (2005) 325–327.

[76] N. Lewinski, V. Colvin, R. Drezek, Cytotoxicity of nanoparticles, Small 4 (1) (2008) 26–49.

[77] G. Vales, S. Suhonen, K. M. Siivola, K. M. Savolainen, J. Catalán, H. Norppa, Genotoxicity and cytotoxicity of gold nanoparticles in vitro: role of surface functionalization and particle size, Nanomaterials 10 (2) (2020) 271.

[78] A. Jaworska, T. Wojcik, K. Malek, U. Kwolek, M. Kepczynski, A. A. Ansary, S. Chlopicki, M. Baranska, Rhodamine 6G conjugated to gold nanoparticles as labels for both SERS and fluorescence studies on live endothelial cells, Microchim. Acta 182 (1-2) (2015) 119–127.

[79] D. Kim, N. Oh, K. Kim, S. Lee, C.-G. Pack, J.-H. Park, Y. K. Park, Label-free high-resolution 3-D imaging of gold nanoparticles inside live cells using optical diffraction tomography, Methods 136 (2018) 160–167.

[80] S. D. Brown, P. Nativo, J.-A. Smith, D. Stirling, P. R. Edwards, B. Venugopal, D. J. Flint, J. A. Plumb, D. Graham, N. J. Wheate, Gold nanoparticles for the improved anticancer drug delivery of the active component of oxaliplatin, J. Am. Chem. Soc. 132 (13) (2010) 4678–4684.

[81] A. N. Dosumu, S. Claire, L. S. Watson, P. M. Girio, S. A. Osborne, Z. Pikramenou, N. J. Hodges, Quantification by luminescence tracking

of red emissive gold nanoparticles in cells, JACS Au 1 (2) (2021) 174–186.

[82] R. B. Elmes, K. N. Orange, S. M. Cloonan, D. C. Williams, T. Gunnlaugsson, Luminescent ruthenium (II) polypyridyl functionalized gold nanoparticles; their DNA binding abilities and application as cellular imaging agents, J. Am. Chem. Soc. 133 (40) (2011) 15862–15865.

[83] P. Nativo, I. A. Prior, M. Brust, Uptake and intracellular fate of surface-modified gold nanoparticles, ACS Nano 2 (8) (2008) 1639–1644.

[84] D. E. Heck, A. M. Vetrano, T. M. Mariano, J. D. Laskin, UVB light stimulates production of reactive oxygen species unexpected role for catalase, Journal of Biological Chemistry 278 (25) (2003) 22432–22436.

[85] R. M. Young, J. K. Arnette, D. A. Roess, B. G. Barisas, Quantitation of fluorescence energy transfer between cell surface proteins via fluorescence donor photobleaching kinetics, Biophys. J. 67 (2) (1994) 881–888.